compounds

MDPI

Article

Magnetron Sputtering as a Solvent-Free Method for Fabrication of Nanoporous ZnO Thin Films for Highly Efficient Photocatalytic Organic Pollution Degradation

Kamila Ćwik [1], Jakub Zawadzki [1,†], Rafał Zybała [1], Monika Ożga [2], Bartłomiej Witkowski [2], Piotr Wojnar [2], Małgorzata Wolska-Pietkiewicz [3], Maria Jędrzejewska [3], Janusz Lewiński [3] and Michał A. Borysiewicz [1,*]

[1] Łukasiewicz Research Network—Institute of Microelectronics and Photonics, Al. Lotników 32/46, 02-668 Warsaw, Poland
[2] Institute of Physics, Polish Academy of Sciences, Al. Lotników 32/48, 02-668 Warsaw, Poland
[3] Faculty of Chemistry, Warsaw University of Technology, Noakowskiego 3, 00-664 Warsaw, Poland; mwolska@ch.pw.edu.pl (M.W.-P.)
* Correspondence: michal.borysiewicz@imif.lukasiewicz.gov.pl
† At time of manuscript submission no longer with the Łukasiewicz Research Network—Institute of Microelectronics and Photonics.

Abstract: Zinc oxide (ZnO) is one of the most versatile semiconductor materials with many potential applications. Understanding the interactions between the surface chemistry of ZnO along with its physico-chemical properties are essential for the development of ZnO as a robust photocatalyst for the removal of aqueous pollutants. We report on the fabrication of nanoparticle-like porous ZnO films and the correlation between the fabrication process parameters, particle size, surface oxygen vacancies (SOV), photoluminescence and photocatalytic performance. The synthesis route is unique, as highly porous zinc layers with nanoscale grains were first grown via magnetron sputtering, a vacuum-based technique, and subsequently annealed at temperatures of 400 °C, 600 °C and 800 °C in oxygen flow to oxidise them to zinc oxide (ZnO) while maintaining their porosity. Our results show that as the annealing temperature increases, nanoparticle agglomeration increases, and thus there is a decrease in the active sites for the photocatalytic reaction. However, for selected samples the annealing leads to an increase of the photocatalytic efficiency, which we explain based on the analysis of defects in the material, based on photoluminescence (PL). PL analysis showed that in the material the transition between the conduction band and the oxygen vacancy is responsible for the green emission centered at 525 nm, but the photocatalytic activity correlated best with surface states—related emission.

Keywords: ZnO nanostructures; photocatalysis; photoluminescence; solvent-less; sputter deposition

Citation: Ćwik, K.; Zawadzki, J.; Zybała, R.; Ożga, M.; Witkowski, B.; Wojnar, P.; Wolska-Pietkiewicz, M.; Jędrzejewska, M.; Lewiński, J.; Borysiewicz, M.A. Magnetron Sputtering as a Solvent-Free Method for Fabrication of Nanoporous ZnO Thin Films for Highly Efficient Photocatalytic Organic Pollution Degradation. *Compounds* **2024**, *4*, 534–547. https://doi.org/10.3390/compounds4030032

Academic Editor: Maria Lurdes Santos Cristiano

Received: 29 July 2024
Revised: 15 August 2024
Accepted: 21 August 2024
Published: 4 September 2024

1. Introduction

Zinc oxide (ZnO) is a wide band-gap semiconductor with a direct band gap (3.35 eV), large exciton binding energy of 60 meV, which can be doped to show a resistivity of 4.4×10^{-3} Ω· cm at room temperature [1–3]. These properties make it of interest as a potential material for applications in gas sensors [4], transistors [5], LEDs [6], photocatalysis [7], ultra-violet lasers [8] and also in solar energy conversion [9]. The controlled derivation of nanoscale shapes and different morphologies is of great interest because of the possibility of tuning the physico-chemical properties of these materials related to their surface properties and states. ZnO nanostructures can be synthesized in a number of ways. Based on the most commonly used approaches we can propose the division to vacuum and chemical methods, both of which have their own advantages and yield different properties of the materials [2,10–12]. The chemical methods focus mainly on obtaining nanostructured ZnO by wet methods such us sonochemical [13], sol-gel [14], solvo- or hydrothermal [15] or

organometallic approaches [16,17], etc, leading to the formation of nanostructures and nanoparticles. Vacuum methods focus more on thin, uniformly dense films grown by means of atomic layer deposition [18] or epitaxial techniques [19], pulsed laser deposition [20] or magnetron sputtering [21].

The magnetron sputtering technique is the one which is the least cost-intensive of the vacuum-based ones. Most of the research on ZnO materials done by sputtering concerns transparent conductive ZnO-based films [8]. In this technique, a substrate is positioned close to the deposition source, where it catches the arriving particles and enables them to coalesce into a layer. Because the procedure takes place in a vacuum deposition chamber, the particles can move about freely. The coatings produced this way are in most cases textured along the substrate-source line of sight, and are not conforming because the particles have a tendency to travel in straight lines. Magnetron sputtering can be used to deposit metals, alloys, and composites on a variety of materials with thickness in the nanometer and micrometer range. Compared to other vacuum coating processes, it has a number of significant advantages shown in Figure 1. These properties have led to the development of many commercial applications, from the production of microelectronics to simple decorative coatings [22,23]. Several years ago, our group showed it was surprisingly possible to obtain ZnO nanostructures through magnetron sputtering with ex-situ post-deposition annealing in oxygen [21] which opened the way for uniform nano-structural ZnO coatings on large surfaces. Their applicability in surface reaction-based applications will be shown here as electrodes for photocatalytic water purifying. Although ZnO can decompose in strongly basic or acidic environments, its low toxicity and availability makes is one of the materials of choice for photocatalysis. The advantage of our fabrication method is that the material grows in the form of a meso-porous structure which enables unrestricted medium flow to the ZnO nano-crystals, as is opposite to the solution-processed material where the spherical nanocrystallites aggregate, reducing their available surface and thus the photocatalytic activity [7,24,25]. This also means that less material is required to achieve the same efficiency. Finally, no wet chemical processing means that no ligands are covering the surface of the nanostructures, make them more available for any surface-bound reactions, such as the ones in photocatalysis. Additionally, annealing is a heat treatment process that often determines the crystal structure, morphology, and chemical properties. Many reports emphasize the importance of annealing and the relationship between the increase in photocatalytic activity and the annealing temperature of the layer, as described by Kim et al. [26]. The high activity of nanocomposites obtained after annealing the seed layer is attributed to their high ability to absorb UV radiation, large surface area, and abundance of oxygen defects, which promote the separation of electron-hole pairs, reducing electron recombination [26,27].

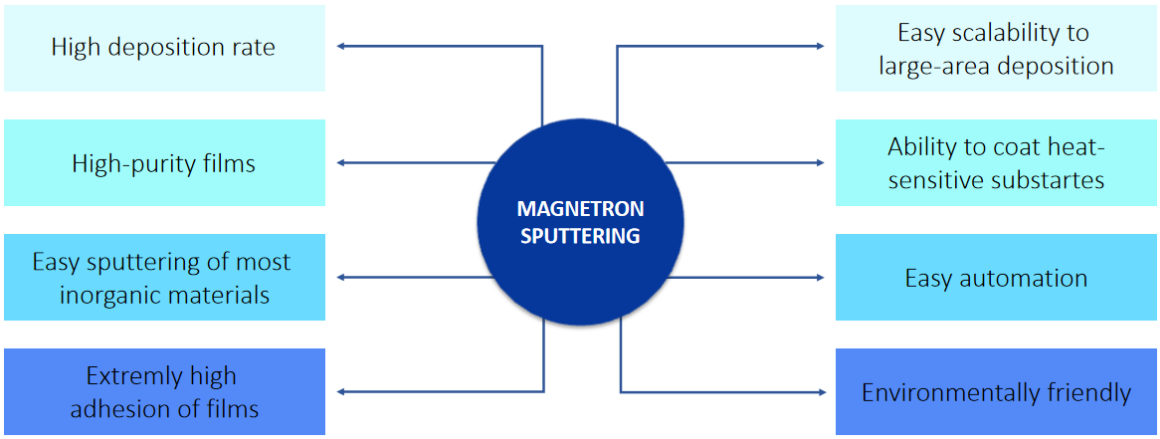

Figure 1. Advantages of magnetron sputtering.

In photocatalysis, the electronic properties of the material play a significant role. ZnO is generally an n-type semiconductor with the presence of defects such as oxygen vacancies (V_O), interstitial zinc ions and zinc vacancies (V_{Zn}), which affect its optical and electrical properties. In particular, the V_O act as donors in ZnO [28], providing additional free electrons to the system, while the V_{Zn} act as acceptors, quenching the conductivity. We will discuss the influence of the defects observed in the material on the photocatalytic efficiency in further parts of the text. A simplified diagram of the heterogeneous oxidation steps in the photocatalytic reaction proceeding with ZnO NPs are shown in Figure 2. The stages of the entire process can be described as follows: (1) diffusion of organic impurities from the liquid phase onto the ZnO surface; (2) adsorption of organic impurities on the ZnO surface; (3) red-ox reaction in the adsorbed phase; (4) desorption of products and (5) removal of products from the interface area [7,29]. The red-ox reaction in this schematic takes place in the presence of UV light through a generation of reactive oxygen species (ROS) (Figure 3). In the presence of radiation with a wavelength less than 400 nm, electrons (e^-) are excited from the valence band (VB) into the conduction band (CB), generating positively charged holes (h^+). In the aquatic environment the photo-generated electron can reduce a dioxygen molecule to form a superoxide radical anion (O_2^-), while h^+ can oxidize water molecules and hydroxide ions, generating hydroxyl radicals and H_2O_2 hydrogen peroxide molecules. In addition, recombination of electron-hole pairs can generate photon emission (radiative recombination), which in turn can excite ground-state oxygen, producing singlet oxygen [30–32]. The combined effects of photodissociation of H_2O_2 in the presence of light and on the surface of the photocatalyst, as well as the complex transport of highly reactive hydroxyl radicals OH· in the reactant mixture, may be responsible for the enhanced photodegradation of MB in the presence of zinc oxide and H_2O_2. During the conversion of these molecules mineral acids, CO_2 and H_2O are produced. The following reaction strategies for the photolysis of H_2O_2 are based on the literature (Figure S1 in the Supplementary Information) [26,33,34]. Based on our previous studies, the annealing conditions applied in the process of fabricating our nanoporous ZnO films can lead to differences in the optically active defect density in the films [35]. Therefore, in the current study, we wanted to explore this concept and look at how the properties of differently deposited and annealed material would influence the photocatalytic activity of nanostructured ZnO thin films during degradation of pollution in water, and discuss the role of the defects in the photocatalytic process.

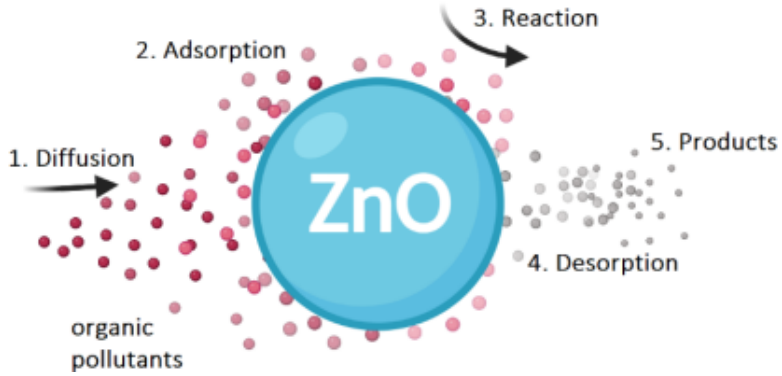

Figure 2. Heterogeneous photocatalytic process steps.

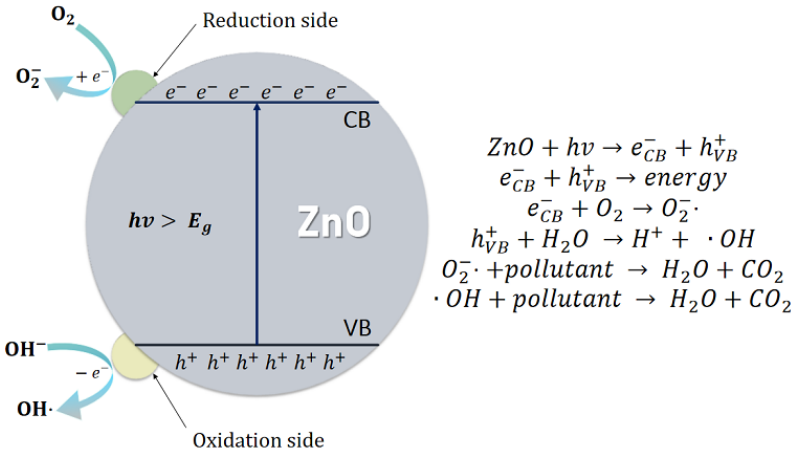

Figure 3. Mechanism of radiation-induced formation of reactive oxygen forms.

2. Materials and Methods

Fabrication Zn/ZnO thin films. The experimental setup for magnetron sputtering deposition is schematically shown in Figure 4. The substrate was Si (100) with a thickness of 500 µm, but in principle it can also be a paper, quartz, glass, metallic, polymer or other substrate. The cleaned and washed silicon wafer was placed in the process chamber of the sputtering device and the chamber was pumped down to a vacuum of 10^{-5} Pa. The deposition involved a combination of oxygen and argon in a set ratio. The gas flows used were 3 sccm Ar: 0.3 sccm O_2—sample A, 3 sccm Ar: 0.6 sccm O_2—sample B, 6 sccm Ar: 0.6 sccm O_2—sample C, and 10 sccm Ar: 1 sccm O_2—sample D. The addition of a small oxygen content to the argon gas leads to the growth of porous films, as the oxygen induces increased nucleation of new grains as well as enables the self-shadowing growth of the porous structures, as discussed in detail elsewhere [36]. The sputtering process itself was carried out using a 75 mm diameter zinc target supplied in DC mode with 80 W DC power, placed at a distance of 15 cm from the silicon wafer.

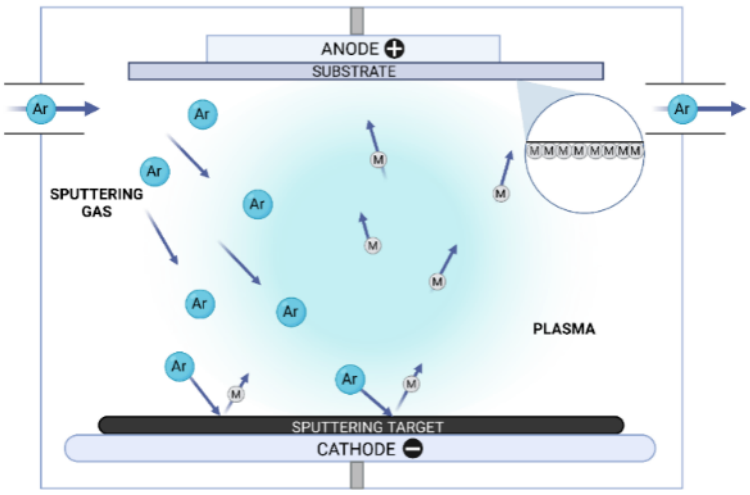

Figure 4. Sputtering deposition setup schematic.

A constant pressure of 0.4 Pa was maintained in the process chamber throughout the entire deposition process, the time of which was varied to get porous zinc films with a profilometer-determined thickness of 1000 nm on the surface of the silicon wafers. This time was equal to: 28 min 37 s, 22 min 46 s, 25 min 25 s and 22 min 19 s respectively for samples A, B, C and D. As the films are porous, their top surface has a significant roughness and the determined thickness is a mean value over a certain distance, as is the case with profilometer measurements. SEM cross-section images of the deposited films

were presented in Figure S2 in the Supplementary Information Since the deposited material is meso-porous nanostructured Zn, it needs to be annealed in oxygen after deposition to form ZnO. Despite the increase in particle size with annealing temperature, the thickness of the films does not change after annealing (see Figure S3 in the Supplementary Information). However, the activity of the photocatalyst is enhanced due to the increased number of defects, extended lifetime of charge carriers and higher quantum yield. The post-deposition annealing process is performed in a dry oxygen flow and the main variable responsible for the outcome is the annealing temperature. We know from previous experiments, that the temperature has to be equal or higher than 400 °C, which is why we chose 400, 600 and 800 °C annealing temperatures for samples from each deposition batch, yielding 12 different samples. The annealing time is 20 min in each case.

2.1. Material Characterization

In order to fully characterize the obtained films, a wide range of studies were carried out. The structural characterization of ZnO thin films were performed by Scanning Electron Microscopy (SEM) on a Zeiss Gemini system (Oberkochen, Germany). The crystal structure was studied by X-ray diffraction (XRD) using an Empyrean diffractometer from Malvern Panalytical (Malvern, UK) equipped with a copper anode X-ray tube with a copper anode as a source of Cu Kα radiation. Measurements were made in Bragg-Brentano geometry, in 2θ range: 20°–80° with a step of 0.0131°. The optical characterization was done using room-temperature photoluminescence (PL) with a Kimmon Koha (Itabashi, Japan) 325 nm He-Cd laser excitation and a Shamrock 500 spectrometer (Andor-Solis, Belfast, Northerm Ireland) using a 600 lines/mm diffraction grating.

2.2. Photocatalysis Measurement

Methylene blue (MB) was the model organic pollutant to examine the ZnO samples photocatalytic activity. These properties were evaluated based on the rate and degree of degradation of MB over time under the influence of UV radiation at room temperature. The decomposition processes were monitored by UV-Vis measurements on the Hitachi (Tokyo, Japan) U-2910 spectrophotometer. A standard 3.5 mL quartz cell (Hellma) with a 10 mm path length and transparent on all four sides was used.Absorption spectra were recorded at intervals of 20 min, with the first 40 min the degradation of the dye took place without the use of UV light (6 W, 365 nm). The typical procedure consisted of the immersion of the 10 mm × 10 mm substrate with a layer of porous ZnO in 10.5 mL MB solution with constant stirring. Work station diagram for photocatalysis is shown in Figure S4 in the Supplementary Information. Photocatalytic activity was assessed by measuring and analyzing UV-Vis spectra after each 20 min up to 240 min total degradation time. The percentage of MB degradation was calculated as follows: $\%_{MBdegradation} = [(C_0 - C)/C_0] \times 100\%$, where C_0 is the initial absorbance, C is the absorbance after irradiation at various time intervals.

3. Results

Below, we present the results of the vacuum approach, i.e., fabrication of thin films porous Zn by magnetron sputtering and post-deposition oxidation at various temperatures to get ZnO, allowing comparative investigation on the preparation and characterization of thin film porous ZnO. In addition, experiments of photocatalytic activity have been carried out to establish the fabrication-property-relationship of the selected ZnO thin films.

3.1. X-ray Diffraction

The XRD analysis of the samples before and after annealing between 400 °C and 800 °C is presented in Figure 5. The major diffraction peaks for Zn were seen in the as-deposited samples. These disappeared after annealing and peaks corresponding to the (100), (002), (101), (102), (110), (103), (200), (112), and (201) ZnO planes were detected at different positions for the analyzed samples for all temperatures and morphologies. This confirms that the material is pure ZnO with the wurtzite hexagonal phase (JCPDS no. 36-1451).

The sharp peaks on the XRD pattern allow to conclude that obtained porous ZnO thin films are highly crystalline. The peak intensity of the (100), (002), and (101) planes increased with increasing annealing at temperatures of 400 °C, 600 °C, and 800 °C indicating improving crystallinity. High crystallinity promotes the transfer of photo generated electrons and holes from the bulk to the surface of the photocatalyst, enhancing photocatalytic efficiency. The only sample with remaining Zn peaks in the pattern after annealing is Sample A annealed at 400 °C suggesting that not all of the Zn layer was oxidized to ZnO and pure zinc remained in the material. The resulting sizes of the crystallites calculated using Scherrer's formula are shown in Table S1 in the Supporting Information. Annealing with an increase in temperature range 400–600 °C promotes agglomeration and coalescence of the nanowires, as was observed for our samples annealed in an oxygen atmosphere.

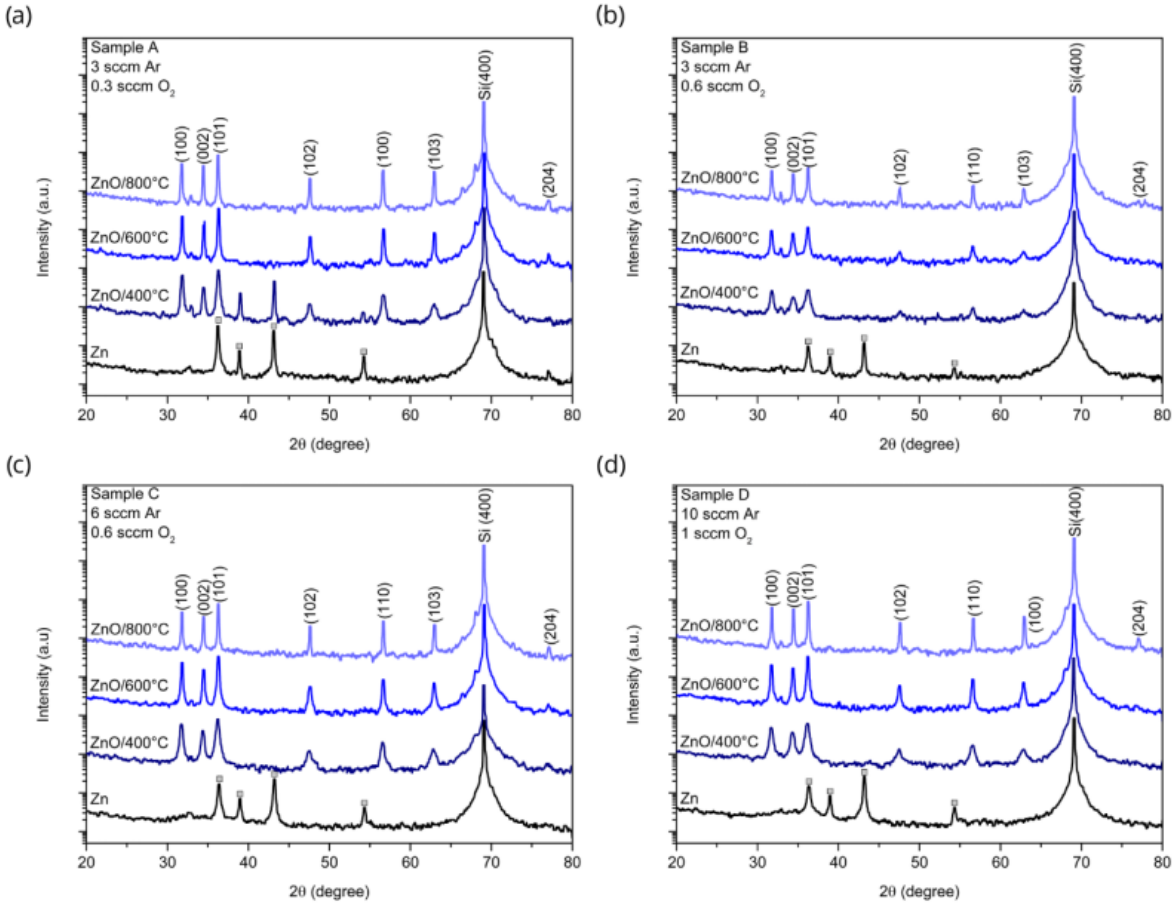

Figure 5. X-ray diffraction (XRD) for porous Zn films before and after annealing in the presence of oxygen for samples A (**a**), B (**b**), C (**c**) and D (**d**). Zn peak positions marked with grey squares.

Consistent with this, increasing the temperature causes the decrease of pore sizes and volume thereby reducing the active surface area of ZnO as a photocatalyst. These results suggest that we can control grain size with annealing temperature.

The SEM images (Figure 6) show that the particle sizes are in the range 50 to 600 nm. The Scherrer equation, however, yields crystallite sizes that are smaller than 44 nm. The SEM gives the particle size but the Scherrer equation gives us the size of the crystallite. In essence, a crystallite is a single crystal. We work with polycrystalline particles, which are made up of many crystallites. As a result, the particle size of a polycrystalline material is larger than its crystallite size. All of the samples presented in this paper appear to be polycrystalline, as evidenced by the many peaks seen in their X-ray diffraction patterns.

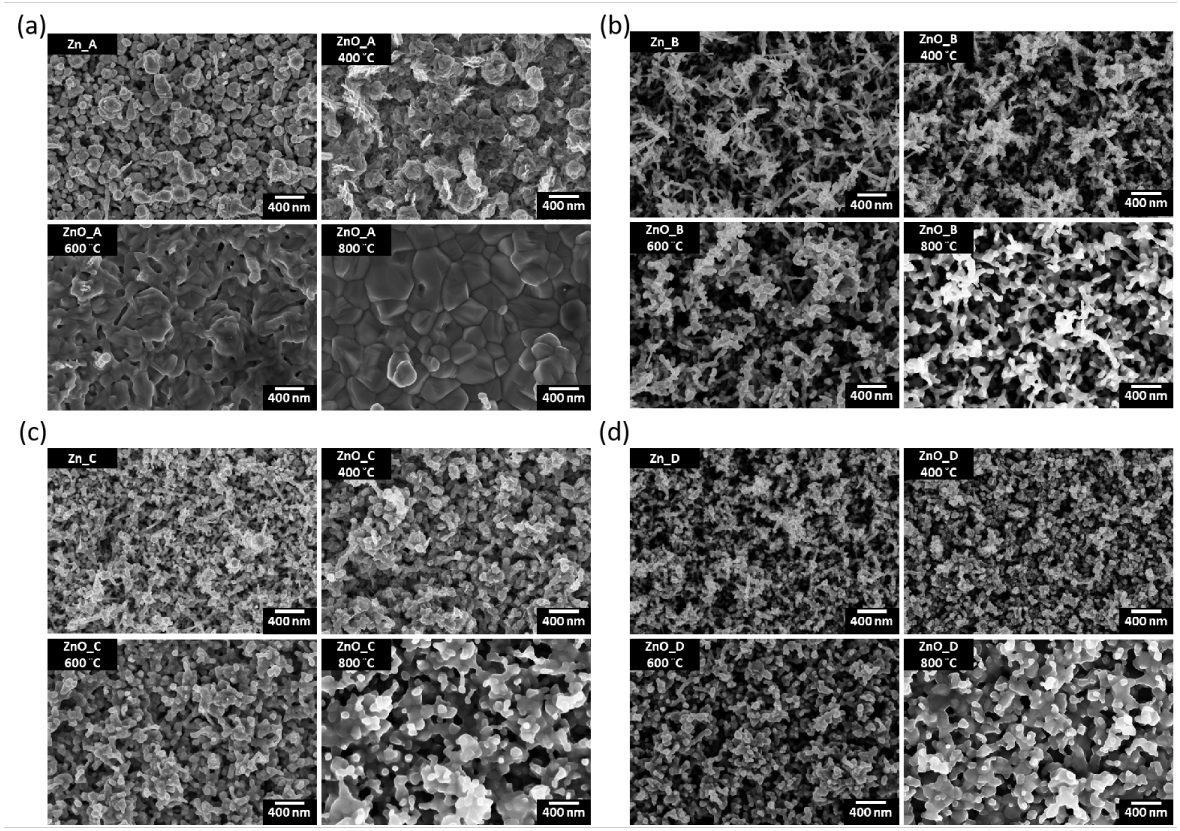

Figure 6. SEM images of zinc and oxidized zinc samples annealed at different temperatures of 400 °C, 600 °C and 800 °C for a zinc sample deposited in flow of (**a**) 3 sccm Ar and 0.3 sccm O_2, (**b**) 3 sccm Ar and 0.6 sccm O_2, (**c**) 6 sccm Ar and 0.6 sccm O_2, (**d**) 10 sccm Ar and 1 sccm O_2.

3.2. Scanning Electron Microscopy

The plan-view images in Figure 6 shows also that the increase in the oxidation temperature of the porous zinc layer causes a change in morphology for each sample from whiskers to more spherical particles. Therefore, agglomeration of the material is observed, which can lead to a decrease in the specific surface area of the film. This phenomenon was observed for all morphologies except samples from batch B, which retained their morphology to a much greater extent than the samples from other batches.

3.3. Optical Properties

Figure 7 illustrates the PL spectra of porous ZnO thin films annealed in oxygen at 400–800 °C. Three distinct areas can be identified in all spectra. Several peaks in the range of 360–390 nm, next a significant broad peak centered at 525 nm and finally a very intensive peak centered around 680–700 nm. On top of the last peak, a second diffraction order of the structure from the 360–390 range is visible.

The UV emission at 360–390 nm, denoted as Near Band Edge Emission (NBE), is related to excitonic recombination at energies close to the ZnO band edge. A clear NBE emission visible at room temperature for all sample batches indicates a the very high crystal quality of the individual nanocrystallites. The dominating NBE lines, can be identified, based on the previous studies of nanoporous ZnO [35] as free excitons (FX) at 3.41 eV and donor-bound excitons (D^0X) at 3.36 eV [37–41]. The lower intensity lines are LO phonon replicas of the D^0X line positioned respectively one (72 meV) and two (144 meV) LO phonon energies in ZnO below the D^0X line [42]. A small peak on the high energy slope of the D^0X line (3.37 eV) in samples annealed at 800 °C can be attributed to the surface bound excitons (SBE) usually visible with samples with a highly developed surface like ours [35]. This peak structure is the same, with same positions of the peaks for all

the sample batches, however the general intensities of the emission are the highest in the batch B-800 °C. The intensity of the near band edge (NBE) UV emission region increases as the annealing temperature was raised from 400 °C to 800 °C, relating to the improved crystalline quality, which is consistent with the XRD data.

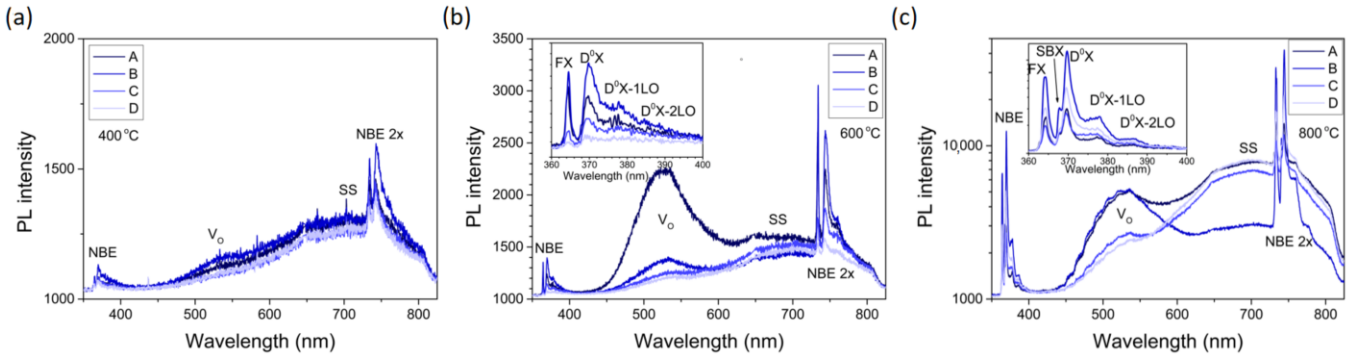

Figure 7. PL spectra of porous ZnO films grown on Si substrate, annealed at (**a**) 400 °C, (**b**) 600 °C and (**c**) 800 °C.

Photoluminescence emission with energies smaller than the ZnO band gap can be related to a number of intrinsic effects of the ZnO crystal including oxygen and zinc vacancies (V_O, V_{Zn}), interstitial atoms (O_i, Zn_i) or anti-site defects (O_{Zn}, Zn_O), as well as various surface states. A schematic of mechanisms for possible visible light emission sources in ZnO thin films is illustrated in Figure S5 in the Supplementary Information. In the measured spectra, the broad peak (FWHM around 0.4 eV) centered around 525 nm giving green emission is very pronounced with its tails reaching the blue region. The green emission can be attributed to the transition between the band-edge and local defect-originating energy levels within the band-gap. It is commonly acknowledged that the transitions responsible for this green emission are between conduction band minimum and oxygen vacancies (V_O) [43]. A second candidate would be intra-gap transitions between extended interstitial zinc levels ($ex - Zn_i$i) and zinc vacancies (V_{Zn}) [44]. Although both Zn_i and V_{Zn} are widely recognized as major defects within the material [42], we do not see any emission related to neither $Zn_i - VB$, $Zn_i - V_{Zn}$ nor $CB - V_{Zn}$ transitions, which should be observed in the violet and blue ranges. This allows us to conclude that the defect responsible for the green emission in our material is the V_O. The broad peak of red luminescence (FWHM of 0.45–0.55 eV), centered at around 700 nm is related to energy levels which is typically attributed to surface-related mid-gap states (SS) of unknown charge [45]. Other possibilities include oxygen vacancies [46] and oxyygen interstitials [47]. It has to be noted, however, that the intensity of this line does not correlate with the green V_O emission, and that in the samples annealed at high temperatures the presence of interstitials is highly unlikely, which is why the surface state identification will be used here. It can be strongly influenced by the processing of the material. The reason for two broad visible bands is that ZnO films have a large surface to volume ratio and high porosity leading to a relatively broad distribution of physical properties of the nanocrystallites. Since the FX and D^0X emissions are strongly related to the energy gap of the material and the crystalline quality, they tend to differ very little between the samples. On the other hand, the distribution of defects and surface states is strongly depended on the material morphology and processing conditions. The latter is also true for the SBX, which appear after annealing at 800 °C.

3.4. Photocatalytic Degradation of Methylene Blue by ZnO Thin Films

Methylene blue is a standard aqueous impurity used to determine the photocatalytic potential of various materials, including ZnO. The spectra of the MB solutions before degradation and after 240 min degradation for all samples along with the trends of degradation as a function of time for all samples are shown in Figure 8. Generally, the higher the oxidation temperature, the better the conversion efficiency (Table S2). The annealing

at 400 °C shows similar MB degradation for samples B, C and D, while for the sample A it shows almost no degradation. The low percentage of methylene blue degradation for sample A annealed at 400 °C may be attributed to incomplete oxidation of the zinc layer, making oxidation under such conditions insufficient to obtain a homogeneous ZnO layer, as shown in the XRD patterns in Figure 6. Increasing the oxidation temperature to 600 °C increases the degradation percentage of MB for all samples, however the increase is the smallest for the sample B. It is worth noting, that samples C and D start to show some degree of ripening while sample A shows agglomeration, with larger crystallites. This does not seem to influence the degradation. Furthermore, heating at a temperature of 800 °C causes a more pronounced ripening of the samples C and D and substantial agglomeration and calcination of the sample A, as shown in SEM images, leading to a reduction in the active surface area of porous layers in the case of the sample A to almost no porosity. This leads to a drop in the degradation efficiency for sample A Sample B, shows other behavior, with no morphology changes visible and an increase in the percentage of degradation.

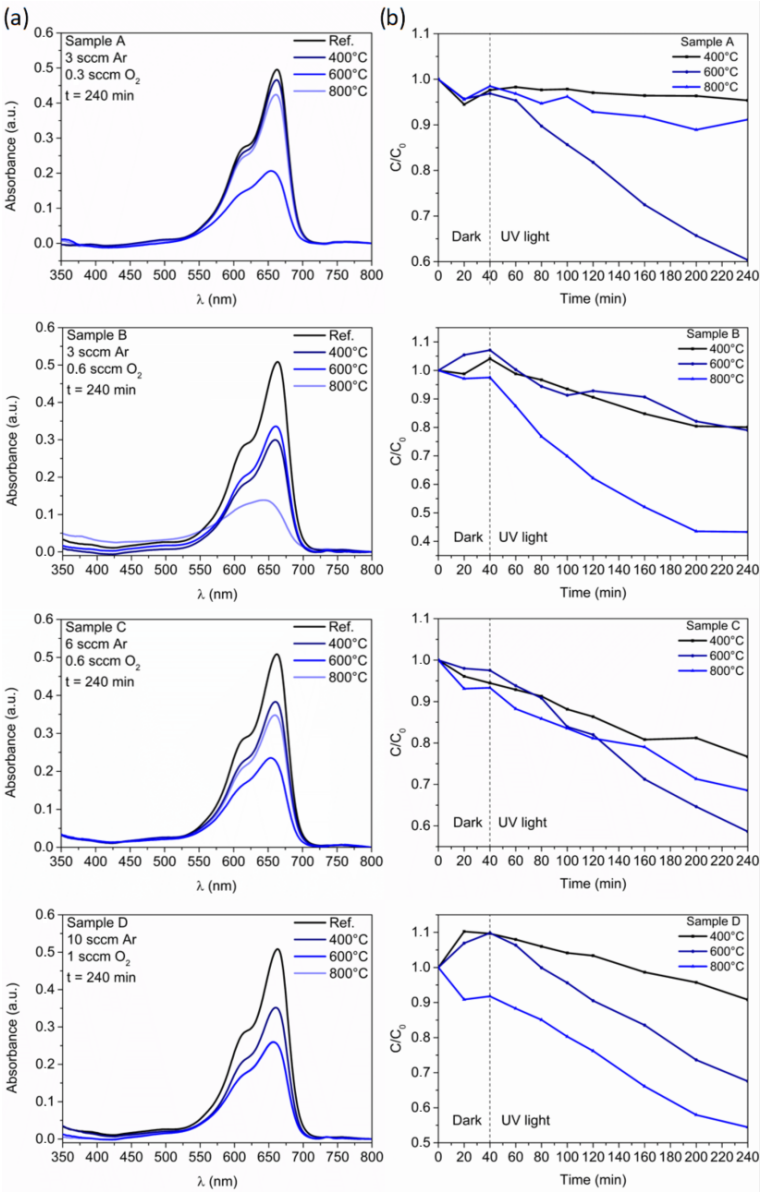

Figure 8. (**a**) Absorbance spectra of methylene blue dye for catalyst-porous ZnO films of different ZnO morphologies annealed at different temperatures, (**b**) photocatalytic degradation efficiency between C/C_0 and the irradiation time of different ZnO morphology.

4. Discussion

The photodegradation of organic dyes in solution is a complex process, depending on a number of factors, such as the available surface area and availability of active sites at the surface of the catalyst. Trying to understand the photodegradation behavior, we analyzed the areas of all photoluminescence lines, fitted using Gaussian profiles, and their combinations, to find correlations with the degradation percentage. Since the luminescence of the samples annealed at 400 °C is very low, we will present the discussion for samples annealed at 600 and 800 °C. Figure 9 presents the trends for the individual lines from the NBE region, the V_O and the SS lines along with the trend for percent of MB degraded. Looking at the data for 800 °C, it seems that the V_O profile well correlates with the degradation profile, which would be argued by some, as the V_O profile intensity has been shown to correlate positively with the photodegradation efficiency [48]. However, taking into account the system we identified in our samples, including NBE, V_O and SS it is evident, that the V_O is not only an acceptor, which would kill any free electron but is also below the energy level of the SS, which would therefore intercept any surface electrons before it got the chance to get to the V_O. This is further supported by the fact that there is no correlation between the V_O and the degradation for the samples annealed at 600 °C. There, the SS line looks as correlated in a very good way. The SS trend is not well correlated for the samples annealed at 800 °C. However, taking account that the surface effects are responsible for the photocatalytic degradation we notice, that for the 800 °C samples another surface-bound feature is visible in the luminescence spectra—the SBX. If we now combine the SBX and SS lines, we get a very good correlation with the degradation trend, except for the sample A. In the case of this sample, we can assume that the much lower degradation efficiency is related to the calcination and loss of porosity, resulting in a significant loss of surface area.

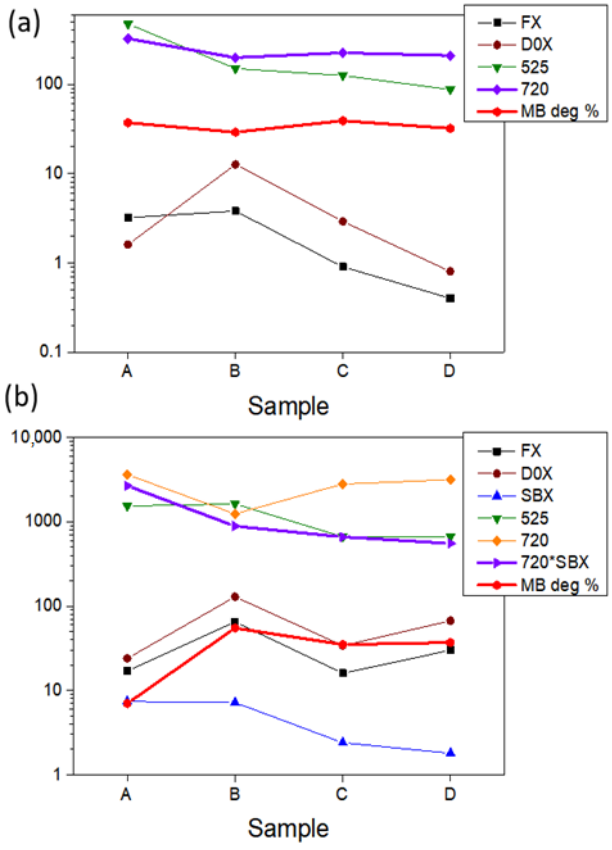

Figure 9. Trends of the photoluminescence line areas and the degradation percentage of MB for the samples annealed at 600 °C (**a**) and 800 °C (**b**).

In order to get more qualitative results, enabling comparison with other approaches, we recalculated the degradation from percent to actuall mass. The typical photocatalytic procedure utilized a 50 mL solution of methylene blue with 50 mg/L, which gives 7.82×10^{-8} moles MB in the volume used, V = 50 mL. Analyses of the deposited ZnO material indicated that 1000 nm of it weighs in the range of 2–77 mg depending on the annealing temperature and deposition parameters. The recalculated values in moles of degraded MB per mass of the ZnO used are shown in Table S3.

A direct comparison to other ZnO nanostructured forms in terms of MB degradation efficiency is possible, but not straightforward, as shown in Table 1. In photocatalysis there is no single standard of neither MB concentration, catalyst loading nor MB solution volume used for the experiment, which requires a discussion of the literature results. Out of the presented data, it can be seen that very high degradation efficiencies are reported for low MB concentration or high catalyst loading, meaning that the ratio of catalyst to the pollutant is high, as one could expect. A high power of the illuminating light also plays a role in increasing the rate of catalysis. These solutions, however lead to the use of a lot of electrical energy and a significant amount of the catalyst material, which in turn generates waste. When comparing with the work of on calcinated ZnO which has the same solution volume and MB concentration, but 25 times higher mass of catalyst and almost 17 times higher illuminating lamp power, we can see that our material in a very small amount, at very small lamp power, yielded a 30%-higher MB degradation. This shows that the efficiency of the developed material is very high and provides better performance than similar materials, while using less power, less chemicals during fabrication and being attached to a rigid surface for ease of handling.

Table 1. Comparison of literature reports on ZnO nanoparticle degradation efficiency of MB, with regard to MB concentration and mass loading of the catalyst.

Catalyst	Light Source	Mass of ZnO (mg)	Volume of Solution (mL)	MB Concentration ($mg \cdot L^{-1}$)	Irradiation Time (min)	MB Degradation (%)	Reference
Sol-gel, sintered 600 °C	Visible	100	100	20	120	25	[49]
Calcinated 700 °C	430 nm, 100 W	10	50	50	120	30.67	[50]
Flame spray pyrolysis	365 nm, 20 W	1500	650	15	60	99	[51]
Multi-shelled decorated	Xenon lamp, 300 W	20	200	10	30	90	[52]
Sample B-800 °C	UVA lamp, 6 W	0.4	50	50	120	40	This work

5. Conclusions

Porous Zn layers with different morphologies were designed and fabricated by sputtering from a Zn target using a DC power source, which were then annealed at different temperatures in the presence of oxygen to obtain porous zinc oxide layers. The effects of annealing on morphology, grain size and photoluminescence and photocatalysis were studied by XRD, SEM, UV-Vis spectrophotometer and PL. The results show that we are able to obtain thin, porous ZnO films with different morphologies, whose grain sizes and optical properties can be controlled by annealing temperature. Studies indicate that there is a strong correlation between the particle size, the PL signal, and therefore the presence of SOV and photocatalytic activity. We explain the activity of the photocatalysis based on the presence of surface-states evident in the photoluminescence. The photocatalytic efficiencies rival those of the nanoparticles, at much lower mass of the active material and without the need for solvent-based processing. Unlike other methods of obtaining ZnO, our method is unique in that it obtains pure material without organic envelopes as is the case in other wet methods, making ZnO thin films promising toward photocatalytic applications as well as beyond.

Supplementary Materials: The following supporting information can be downloaded at: https://www.mdpi.com/article/10.3390/compounds4030032/s1, Figure S1: Mechanism of photolysis of hydrogen peroxide. Figure S2: SEM cross-section images of samples A, B, C and D. Figure S3: SEM cross-section of sample C as-deposited and after annealing showing no significant change in thickness. Figure S4: Schematic drawing of the photocatalysis stand. Figure S5: Mechanism for visible emission of ZnO thin films. Table S1: Comparison of the core size of the obtained ZnO thin films. Table S2: Comparison of methylene blue percentages degradation over time for catalysts—porous ZnO films with different morphologies annealed at different temperatures. Table S3: Comparison of photocatalysis efficiency methylene blue on 1 mg photocatalyst—ZnO thin films with different morphologies annealed at different temperatures.

Author Contributions: Conceptualization, K.Ć. and M.A.B.; methodology, K.Ć., M.W.-P., B.W. and M.A.B.; validation, K.Ć. and M.A.B.; formal analysis, K.Ć., M.W.-P. and M.A.B.; investigation, K.Ć., J.Z., M.O. and M.J.; resources, R.Z., B.W., P.W. and J.L.; data curation, K.Ć.; writing—original draft preparation, K.Ć.; writing—review and editing, M.A.B.; visualization, K.Ć.; supervision, M.A.B.; project administration, M.A.B.; funding acquisition, J.L. and M.A.B. All authors have read and agreed to the published version of the manuscript.

Funding: This research was supported by the National Science Centre, Poland, under Grant number UMO 2020/39/D/ST5/01474. This work was also supported by the National program "Doktorat Wdrożeniowy" funded by the Ministry of Science and Higher Education of the Republic of Poland (K.Ć.). This research was cofunded by POB Technologie Materiałowe of Warsaw University of Technology within the Excellence Initiative: Research University (IDUB) programme (M.W.-P., M.J.).

Institutional Review Board Statement: Not applicable.

Informed Consent Statement: Not applicable.

Data Availability Statement: The original contributions presented in the study are included in the article, further inquiries can be directed to the corresponding author.

Conflicts of Interest: The authors declare no conflicts of interest.

References

1. Kolodziejczak-Radzimska, A.; Jesionowski, T. Zinc Oxide-from Synthesis to Application: A Review. *Materials* **2014**, *7*, 2833–2881. [CrossRef] [PubMed]
2. Muslih, E.Y.; Kim, K.H. Preparation of Zinc Oxide (ZnO) Thin Film as Transparent Conductive Oxide (TCO) from Zinc Complex Compound on Thin Film Solar Cells: A Study of O_2 Effect on Annealing Process. *IOP Conf. Ser. Mater. Sci. Eng.* **2017**, *214*, 012001. [CrossRef]
3. Khranovskyy, V.; Yakimova, R. Morphology Engineering of ZnO Nanostructures. *Phys. Condens. Matter* **2012**, *407*, 1533–1537. [CrossRef]
4. Kang, Y.; Yu, F.; Zhang, L.; Wang, W.; Chen, L.; Li, Y. Review of ZnO-Based Nanomaterials in Gas Sensors. *Solid State Ionics* **2021**, *360*, 115544. [CrossRef]
5. Alshammari, F.H.; Nayak, P.K.; Wang, Z.; Alshareef, H.N. Enhanced ZnO Thin-Film Transistor Performance Using Bilayer Gate Dielectrics. *ACS Appl. Mater. Interfaces* **2016**, *8*, 22751–22755. [CrossRef] [PubMed]
6. Fan, J.C.; Sreekanth, K.M.; Xie, Z.; Chang, S.L.; Rao, K.V. P-Type ZnO materials: Theory, growth, properties and devices. *Prog. Mater. Sci.* **2013**, *6*, 874–985. [CrossRef]
7. Kulis-Kapuscinska, A.; Kwoka, M.; Borysiewicz, M.A.; Wojciechowski, T.; Licciardello, N.; Sgarzi, M.; Cuniberti, G. Photocatalytic Degradation of Methylene Blue at Nanostructured ZnO Thin Films. *Nanotechnology* **2023**, *34*, 155702. [CrossRef]
8. Mitra, A.; Thareja, R.K.; Ganesan, V.; Gupta, A.; Sahoo, P.K.; Kulkarni, V.N. Synthesis and Characterization of ZnO Thin Films for UV Laser. *Appl. Surf. Sci* **2001**, *174*, 232–239. [CrossRef]
9. Ameen, S.; Akhtar, M.S.; Song, M.; Shin, H.S. Vertically Aligned ZnO Nanorods on Hot Filament Chemical Vapor Deposition Grown Graphene Oxide Thin Film Substrate: Solar Energy Conversion. *ACS Appl. Mater. Interfaces* **2012**, *4*, 4405–4412. [CrossRef]
10. Johari, S.; Muhammad, N.Y.; Zakaria, M.R. Study of Zinc Oxide Thin Film Characteristics. *EPJ Web Conf.* **2017**, *162*, 01057. [CrossRef]
11. Etcheverry, L.P.; Flores, W.H.; da Silva, D.L.; Moreira, E.C. Annealing Effects on the Structural and Optical Properties of ZnO Nanostructures. *Mater. Res.* **2018**, *21*, e20170936. [CrossRef]
12. Agrawal, S.; Rane, R.; Mukherjee, S. ZnO Thin Film Deposition for TCO Application in Solar Cell. *Conf. Pap. Energy* **2013**, *2013*, 718692. [CrossRef]

13. Kumar, V.; Gohain, M.; Kant, R.; Ntwaeaborwa, O.M.; Hari, P.; Swart, H.C.; Dutta, V. Annealing Induced Oxygen Defects on Green Sonochemically Synthesized ZnO Nanoparticles for Photoelectrochemical Water Splitting. *ChemistrySelect* **2018**, *3*, 11914–11921. [CrossRef]
14. Olejnik-Fehér, N.; Jędrzejewska, M.; Wolska-Pietkiewicz, M.; Lee, D.; De Paëpe, G.; Lewiński, J. On the Fate of Lithium Ions in Sol–Gel Derived Zinc Oxide Nanocrystals. *Small* **2024**, *20*, 2309984. [CrossRef] [PubMed]
15. Mohan, S.; Vellakkat, M.; Aravind, A.; Reka, U. Hydrothermal synthesis and characterization of Zinc Oxide nanoparticles of various shapes under different reaction conditions. *Nano Express* **2020**, *1*, 030028. [CrossRef]
16. Wolska-Pietkiewicz, M.; Tokarska, K.; Grala, A.; Wojewódzka, A.; Chwojnowska, E.; Grzonka, J.; Cywiński, P.J.; Kruczała, K.; Sojka, Z.; Chudy, M.; et al. Safe-by-Design Ligand-Coated ZnO Nanocrystals Engineered by an Organometallic Approach: Unique Physicochemical Properties and Low Toxicity toward Lung Cells. *Chem. Eur. J.* **2018**, *24*, 4033–4042. [CrossRef]
17. Jędrzejewska, M.; Wolska-Pietkiewicz, M.; Drużyński, Z.; Lewiński, J. Organometallic One-Pot Synthesis of ZnO Quantum Dots Coated by Sulfoxides as L-Type Ligands. *J. Mater. Chem. C* **2023**, *11*, 15016–15029. [CrossRef]
18. Tynell, T.; Karppinen, M. Atomic Layer Deposition of ZnO: A Review. *Semicond. Sci. Technol.* **2014**, *29*, 043001. [CrossRef]
19. Triboulet, R.; Perrière, J. Epitaxial Growth of ZnO Films. *Prog. Cryst. Growth Charact. Mater.* **2003**, *47*, 65–138. [CrossRef]
20. Yudasari, N.; Kennedy, D.S.; Suliyanti, M.M. Pulse Laser Deposition (PLD) Technique for ZnO Photocatalyst Fabrication. *J. Phys. Conf. Ser.* **2019**, *1191*, 012009. [CrossRef]
21. Borysiewicz, M.A.; Dynowska, E.; Kolkovsky, V.; Dyczewski, J.; Wielgus, M.; Kamińska, E.; Piotrowska, A. From Porous to Dense Thin ZnO Films through Reactive DC Sputter Deposition onto Si (100) Substrates. *Phys. Status Solidi Appl. Mater. Sci.* **2012**, *209*, 2463–2469. [CrossRef]
22. Tudose, I.V.; Comanescu, F.; Pascariu, P.; Bucur, S.; Rusen, L.; Iacomi, F.; Koudoumas, E.; Suchea, M.P. Chemical and Physical Methods for Multifunctional Nanostructured Interface Fabrication. In *Functional Nanostructured Interfaces for Environmental and Biomedical Applications*; Elsevier: Amsterdam, The Netherlands, 2019; pp. 15–26.
23. Kwoka, M.; Lyson-Sypien, B.; Kulis, A.; Maslyk, M.; Borysiewicz, M.A.; Kaminska, E.; Szuber, J. Surface Properties of Nanostructured, Porous ZnO Thin Films Prepared by Direct Current Reactive Magnetron Sputtering. *Materials* **2018**, *11*, 131. [CrossRef] [PubMed]
24. Wan, Q.; Wang, T.H.; Zhao, J.C. Enhanced Photocatalytic Activity of ZnO Nanotetrapods. *Appl. Phys. Lett.* **2005**, *87*, 083105. [CrossRef]
25. Tran, T.H.; Tran, T.N.A.; Bach, T.C.; Sai, C.D.; Pham, N.H.; Tran, V.T.; Nguyen, T.B.; Nguyen, Q.H.; Pham, V.T.; Doan, Q.K.; et al. Effect of annealing on the properties of transparent conducting Ag doped ZnO thin films prepared by r.f. magnetron sputtering method. *Micro Nanostruct.* **2022**, *166*, 207219. [CrossRef]
26. Kim, W.Y.; Kim, S.W.; Yoo, D.H.; Kim, E.J.; Hahn, S.H. Annealing Effect of ZnO Seed Layer on Enhancing Photocatalytic Activity of ZnO/TiO_2 Nanostructure. *Int. J. Photoenergy* **2013**, *2013*, 130541. [CrossRef]
27. Suguna, A.; Prabhu, S.; Selvaraj, M.; Geerthana, M.; Silambarasan, A.; Navaneethan, M.; Ramesh, R.; Sridevi, C. Annealing Effect on Photocatalytic Activity of ZnO Nanostructures for Organic Dye Degradation. *J. Mater. Sci. Mater. Electron.* **2022**, *33*, 8868–8879. [CrossRef]
28. Janotti, A.; Van De Walle, C.G. Native point defects in ZnO. *Phys. Rev. B* **2007**, *76*, 165202. [CrossRef]
29. Ong, C.B.; Ng, L.Y.; Mohammad, A.W. A Review of ZnO Nanoparticles as Solar Photocatalysts: Synthesis, Mechanisms and Applications. *Renew. Sustain. Energy Rev.* **2018**, *81*, 536–551. [CrossRef]
30. Ancona, A.; Dumontel, B.; Garino, N.; Demarco, B.; Chatzitheodoridou, D.; Fazzini, W.; Engelke, H.; Cauda, V. Lipid-Coated Zinc Oxide Nanoparticles as Innovative ROS-Generators for Photodynamic Therapy in Cancer Cells. *Nanomaterials* **2018**, *8*, 143. [CrossRef]
31. Saravanan, R.; Gupta, V.K.; Narayanan, V.; Stephen, A. Comparative Study on Photocatalytic Activity of ZnO Prepared by Different Methods. *J. Mol. Liq.* **2013**, *181*, 133–141. [CrossRef]
32. Mohamed, K.M.; Benitto, J.J.; Vijaya, J.J.; Bououdina, M. Recent Advances in ZnO-Based Nanostructures for the Photocatalytic Degradation of Hazardous, Non-Biodegradable Medicines. *Crystals* **2023**, *13*, 329. [CrossRef]
33. Saha, D.; Desipio, M.M.; Hoinkis, T.J.; Smeltz, E.J.; Thorpe, R.; Hensley, D.K.; Fischer-Drowos, S.G.; Chen, J. Influence of hydrogen peroxide in enhancing photocatalytic activity of carbon nitride under visible light: An insight into reaction intermediates. *J. Environm. Chem. Eng.* **2018**, *6*, 4927–4936. [CrossRef]
34. Pędziwiatr, P.; Mikołajczyk, F.; Zawadzki, D.; Mikołajczyk, K.; Bedka, A. Decomposition of hydrogen peroxide—Kinetics and review of chosen catalysts. *Acta Innov.* **2018**, *26*, 45–52. [CrossRef]
35. Borysiewicz, M.A.; Wzorek, M.; Wojciechowski, T.; Wojtowicz, T.; Kamińska, E.; Piotrowska, A. Photoluminescence of nanocoral ZnO films. *J. Lumin.* **2014**, *147*, 367–371. [CrossRef]
36. Masłyk, M.; Borysiewicz, M.A.; Wzorek, M.; Wojciechowski, T.; Kwoka, M.; Kamińska, E. Influence of absolute argon and oxygen flow values at a constant ratio on the growth of Zn/ZnO nanostructures obtained by DC reactive magnetron sputtering. *Appl. Surf. Sci.* **2016**, *389*, 287–293. [CrossRef]
37. Nizar, B.M.; Lajnef, M.; Chaste, J.; Chtourou, R.; Herth, E. Highly C-Oriented (002) Plane ZnO Nanowires Synthesis. *RSC Adv.* **2023**, *13*, 15077–15085. [CrossRef]
38. Wei, X.Q.; Zhang, Z.G.; Liu, M.; Chen, C.S.; Sun, G.; Xue, C.S.; Zhuang, H.Z.; Man, B.Y. Annealing Effect on the Microstructure and Photoluminescence of ZnO Thin Films. *Mater. Chem. Phys.* **2007**, *101*, 285–290. [CrossRef]

39. Zeng, H.; Duan, G.; Li, Y.; Yang, S.; Xu, X.; Cai, W. Blue Luminescence of ZnO Nanoparticles Based on Non-Equilibrium Processes: Defect Origins and Emission Controls. *Adv. Funct. Mater.* **2010**, *20*, 561–572. [CrossRef]
40. Shen, H.; Shi, X.; Wang, Z.; Hou, Z.; Xu, C.; Duan, L.; Zhao, X.; Wu, H. Defects Control and Origins of Blue and Green Emissions in Sol-Gel ZnO Thin Films. *Vacuum* **2022**, *202*, 111201. [CrossRef]
41. Hsieh, P.T.; Chin, H.S.; Chang, P.K.; Wang, C.M.; Chen, Y.C.; Houng, M.P. Effects of the Annealing Environment on Green Luminescence of ZnO Thin Films. *Phys. B Condens. Matter* **2010**, *405*, 2526–2529. [CrossRef]
42. Janotti, A.; Van de Walle, C.G. Fundamentals of ZnO as a semiconcutor. *Rep. Prog. Phys.* **2009**, *72*, 126501. [CrossRef]
43. Leiter, F.H.; Alves, H.R.; Hofstaetter, A.; Hofmann, D.M.; Meyer, B.K. The Oxygen Vacancy as the Origin of a Green Emission in Undoped ZnO. *Phys. Status Solidi* **2001**, *226*, R4–R5. [CrossRef]
44. Lv, J.; Li, C. Evidences of V_O, V_Zn, and O_i defects as the green luminescence origins in ZnO. *Appl. Phys. Lett.* **2013**, *103*, 232114. [CrossRef]
45. Teklemichael, S.T.; McCluskey, M.D. Acceptor and surface states of ZnO nanocrystals: A unified model. *Nanotechnology* **2011**, *22*, 475703. [CrossRef] [PubMed]
46. Galdámez-Martinez, A.; Santana, G.; Güell, F.; Martínez-Alanis, P.R.; Dutt, A. Photoluminescence of ZnO Nanowires: A Review. *Nanomaterials* **2020**, *10*, 857. [CrossRef] [PubMed]
47. Kumar, V.; Swart, H.C.; Ntwaeaborwa, O.M.; Kroon, R.E.; Terblans, J.J.; Shaat, S.K.K.; Yousif, A.; Duvenhage, M.M. Origin of the red emission in zinc oxide nanophosphors. *Mater. Lett.* **2013**, *101*, 57–60. [CrossRef]
48. Willander, M.; Nur, O.; Sadaf, J.R.; Qadir, M.I.; Zaman, S.; Zainelabdin, A.; Bano, N.; Hussain, I. Luminescence from Zinc Oxide Nanostructures and Polymers and Their Hybrid Devices. *Materials* **2010**, *3*, 2643–2667. [CrossRef]
49. Neena, D.; Kondamareddy, K.K.; Bin, H.; Lu, D.; Kumar, P.; Dwivedi, R.K.; Pelenovich, V.O.; Zhao, X.Z.; Gao, W.; Fu, D. Enhanced visible light photodegradation activity of RhB/MB from aqueous solution using nanosized novel Fe-Cd co-modifed ZnO. *Sci. Rep.* **2018**, *8*, 10691.
50. Ferreira, N.S.; Sasaki, J.M.; Silva, R.S., Jr.; Attah-Baah, J.M.; Macêdo, M.A. Visible-Light-Responsive Photocatalytic Activity Significantly Enhanced by Active [$V_{Zn+}V_{O+}$] Defects in Self-Assembled ZnO Nanoparticles. *Inorg. Chem.* **2021**, *60*, 4475–4496. [CrossRef]
51. Jang, Y.J.; Simer, C.; Ohm, T. Comparison of zinc oxide nanoparticles and its nano-crystalline particles on the photocatalytic degradation of methylene blue. *Mater. Res. Bull.* **2006**, *41*, 67–77. [CrossRef]
52. Song, S.; Wu, K.; Wu, H.; Guo, J.; Zhang, L. Multi-shelled ZnO decorated with nitrogen and phosphorus co-doped carbon quantum dots: Synthesis and enhanced photodegradation activity of methylene blue in aqueous solutions. *RSC Adv.* **2019**, *9*, 7362–7374. [CrossRef] [PubMed]